ORIGINAL PAPER

Corrosion inhibition of mild steel in acidic medium by poly (aniline-co-*o*-toluidine) doped with *p*-toluene sulphonic acid

Varsha Srivastava · M. M. Singh

Abstract The corrosion behaviour of mild steel in 0.5 M H_2SO_4 solution containing various concentrations of a *p*-toluene sulphonic acid doped copolymer formed between aniline and *o*-toluidine was investigated using weight loss, polarization and electrochemical impedance techniques. The copolymer acted as an effective corrosion inhibitor for mild steel in sulphuric acid medium. The inhibition efficiency has been found to increase with increase in inhibitor concentration, solution temperature and immersion time. Various parameters like E_a for corrosion of mild steel in presence of different concentrations of inhibitor and ΔG_{ads}, ΔH^0, ΔS^0 for adsorption of the inhibitor, revealed a strong interaction between inhibitor and mild steel surface. The adsorption of this inhibitor on the mild steel surface obeyed the Langmuir adsorption equation.

Keywords Mild steel · EIS · SEM · Weight loss · Acid inhibition

1 Introduction

The study of corrosion prevention by the use of inhibitors is a matter of high scientific as well as technological importance since it is inexpensive and involves rather simple methodology. Acids are frequently used in many operations such as pickling, cleaning, descaling etc. In order to prevent the attack of the base metal during these processes, corrosion inhibitors are widely employed [1–5]. Organic compounds containing nitrogen, sulphur and oxygen as hetero atoms and delocalized π-electrons have long been recognized as good inhibitors [6–8]. Their role as a physical barrier preventing the access of corrosive environment on the metal surface is well known. The inhibitive effect of nitrogen-containing compounds such as aliphatic amines [9], aniline and alkyl amines [10], *p*-substituted anilines [11] and *o*-substituted anilines [12] is attributed to the formation of a co-ordination bond between iron and nitrogen. The efficacy of using an organic compound as an inhibitor depends firstly, on its ability to get adsorbed on the metal surface and secondly on the effective surface area covered by the inhibitor. The adsorption of these compounds is influenced by the surface charge on the metal and the properties of inhibitor molecules such as electronic structure, type of functional groups, steric factors, aromaticity etc. The dependence of inhibition efficiency on molecular size [13] and molecular weight [14] of the organic molecule is also well established. Thus, by modifying any of these properties their inhibitive properties can be improved.

In recent years, conducting polymers have attracted a lot of attention because of their wide range of industrial applications and economic viability. Polymers possess long chain carbon linkages and therefore, upon adsorption are able to block large areas of the corroding metal surface. The film adsorbed on the metal provides a barrier between the metal and its environment. Due to the extensive delocalization of π-electrons, these polymers could serve as better corrosion inhibitors at very low concentrations, compared to simple organic molecules. Substituted and unsubstituted polyanilines (PANI) [15, 16], poly (aminoquinone) [17], and poly (diphenylamine) [18] have been reported for their corrosion inhibition properties due to the presence of delocalized π-electrons, quaternary nitrogen atoms and large molecular size which ensures greater

V. Srivastava · M. M. Singh (✉)
Department of Applied Chemistry, Institute of Technology, Banaras Hindu University, Varanasi 221005, India
e-mail: mmsingh.apc@itbhu.ac.in

coverage of metallic surface. Poly (aniline-co-metanilic acid) [19] and poly (styrenesulphonic acid) doped polyaniline [20] have been used as inhibitor for mild steel in HCl.

In this paper, the inhibitive action of a synthetic copolymer poly (aniline-co-o-toluidine) doped with p-toluene sulphonic acid (PAT-TSA) on the corrosion of mild steel in sulphuric acid has been investigated. The inhibition efficiency has been evaluated by weight loss, Tafel extrapolation and electrochemical impedance spectroscopic methods. An attempt has been made to establish the mechanism of inhibition from the data thus obtained.

2 Experimental

2.1 Materials

Analytical reagent grade chemicals and monomers (aniline and o-toluidine) were used for the preparation of the copolymer. The copolymerization was carried out by chemical oxidative polymerization using aqueous ammonium persulphate as the oxidizing agent. The concentrations of aniline and o-toluidine were 0.1 mol each and that of HCl was 1.0 mol. The polymerization was initiated by dropwise addition of 0.1 M ammonium persulphate solution. The copolymerization was performed at 0 °C for a period of 4–6 h. The synthesized copolymer was isolated from the reaction mixture by filtration and washed with distilled water to remove the oxidant and oligomers. The synthesized powder was treated with 0.1 M ammonium hydroxide and stirred for 2 h to remove chloride ions which may be present as a dopant in the copolymer. The undoped copolymer was treated with 1.0 mol of p-toluene sulphonic acid in distilled water after stirring at room temperature for 3–4 h. The doped copolymer thus obtained was collected by filtration followed by drying at 50 °C in a thermostatic oven. The molecular weight as measured by Gel Permeation Chromatography (GPC) for the doped copolymer (PAT-TSA) was found to be 11,000.

Analytical reagent grade H_2SO_4 was used for preparation of the test solution. Mild steel samples having percentage composition: C, 0.23; Mn, 0.11; Si, 0.02; P, 0.02; S, 0.02; Ni, 0.02; Cu, 0.01; Cr, 0.01; Fe, remainder, were used as test specimens.

2.2 Characterisation of doped poly (aniline-co-o-toluidine)

The characterization of the synthesized poly (aniline-co-o-toluidine) doped with p-toluene sulphonic acid was carried out by Fourier Transform Infrared (Thermo Nicolet 5700 FTIR spectrometer) spectroscopy.

2.3 Procedure

Weight loss experiments were carried out in a 250 ml beaker kept at the desired temperature in an air thermostat. The steel specimens of size ($4 \times 3 \times 0.1$ cm^3) were dipped in 150 ml of the solution. The test solution consisted of 0.5 M H_2SO_4 with 1, 5, 10, 50, 100, 150, 200 ppm of the synthesized copolymer dissolved in it. The tests were performed for durations between 3 and 72 h at 25 °C with selective concentrations of 1 and 100 ppm and for 24 h at all the concentrations of PAT-TSA over the temperature range 25–65 °C. At the end of the tests, the specimens were carefully washed with water, degreased with acetone and then weighed. Triplicate experiments were performed in each case and the mean value of the weight has been reported. The weight loss data allowed the calculation of the mean corrosion rate in mg cm^{-2} h^{-1}. The % inhibition efficiency has been calculated using the relation [21];

$$\%IE = \frac{CR^0 - CR}{CR^0} \times 100, \tag{1}$$

where CR and CR^0 are the corrosion rates with and without copolymer, respectively.

The electrochemical experiments were done using a conventional three-electrode cell assembly at the selected temperatures. All the solutions were prepared using AR grade chemicals in double distilled water. The mild steel electrode of size ($3 \times 1 \times 0.1$ cm^3) with an exposed area of 1 cm^2 and the rest being covered with extra pure paraffin wax was used as the working electrode. The cell consisted of a platinum counter electrode and a silver/silver chloride electrode as the reference electrode. The working electrode was polished successively with different grades of emery paper (320–2000), washed with water and then degreased with acetone. All the tests were performed under unstirred conditions without deaeration. The polarization and impedance studies were performed using CHI Electrochemical Analyzer (Model 604A). The working electrode was immersed in the acid solution and the constant steady-state (open circuit) potential was recorded when it became virtually constant. The polarization studies were carried out over a potential of +250 to −250 mV with respect to the open circuit potential at a scan rate of 0.5 mV s^{-1}. The linear Tafel segments of the anodic and cathodic curves were extrapolated to obtain corrosion potential (E_{corr}) and corrosion current density (I_{corr}). The inhibition efficiency was evaluated from the measured I_{corr} with and without inhibitor using the relationship,

$$\%IE = \frac{I_{corr}^0 - I_{corr}}{I_{corr}^0} \times 100 \tag{2}$$

where I_{corr}^0 is the corrosion current density without inhibitor and I_{corr} is the corrosion current density with inhibitor.

The polarization resistance (R_p) values were obtained by performing polarization experiments over the potential range $E_{corr} \pm 10$ mV with the scan rate of 0.1 mV s^{-1}. The slope of overpotential (η) versus current density (i) curves yielded the value of R_p. From the measured polarization resistance values, the inhibition efficiency has been calculated using the relationship;

$$\%IE = \frac{R_p - R_p^0}{R_p} \times 100 \qquad (3)$$

where R_p^0 and R_p are the polarization resistance in the absence and in the presence of the inhibitor, respectively.

The impedance measurements were carried out using AC signals of 5 mV amplitude for the frequency spectrum from 100 kHz to 0.01 Hz. The Nyquist representations of the impedance data were analysed with Zsimpwin software. The electrode was kept immersed for half an hour in the solution before starting the impedance measurements. The charge transfer resistance (R_{ct}), was obtained from the diameter of the semicircle of the Nyquist plot. The inhibition efficiency of the inhibitor has been found out from the charge transfer resistance values using the following equation [21–24]:

$$\%IE = \frac{R_{ct} - R_{ct}^0}{R_{ct}} \times 100 \qquad (4)$$

where R_{ct}^0 and R_{ct} are the charge transfer resistance in the absence and in the presence of the inhibitor. The interfacial double layer capacitance (C_{dl}) values were obtained by determining the frequencies at which the imaginary component of the impedance is maximum f ($-Z''_{max}$), using the following equation:

$$C_{dl} = \frac{1}{2\pi \cdot f(-Z''_{max})R_{ct}} \qquad (5)$$

3 Results and discussion

3.1 Infrared spectroscopy

There are a handful of previously published reports discussing the results of infrared spectroscopy of both chemically and electrochemically synthesized polyaniline (PANI) [25, 26] and poly (o-toluidine) doped with mineral as well as functionalized organic acids [27–29]. Figure 1 shows the FTIR spectra of the PAT-TSA synthesized in the laboratory. In general, with some exceptions, the spectral characteristics of the PAT-TSA show greater similarity to the IR spectrum of POT (poly o-toluidine). The band at 1461 cm^{-1} of PANI, attributed to the aromatic ring C–C stretching mode is blue shifted to 1484 cm^{-1} for POT, whereas this mode for PAT-TSA appears in the 1478–1486 cm^{-1} range. The out of plane –NH bending vibration of PANI at 1296 cm^{-1} is absent in the IR
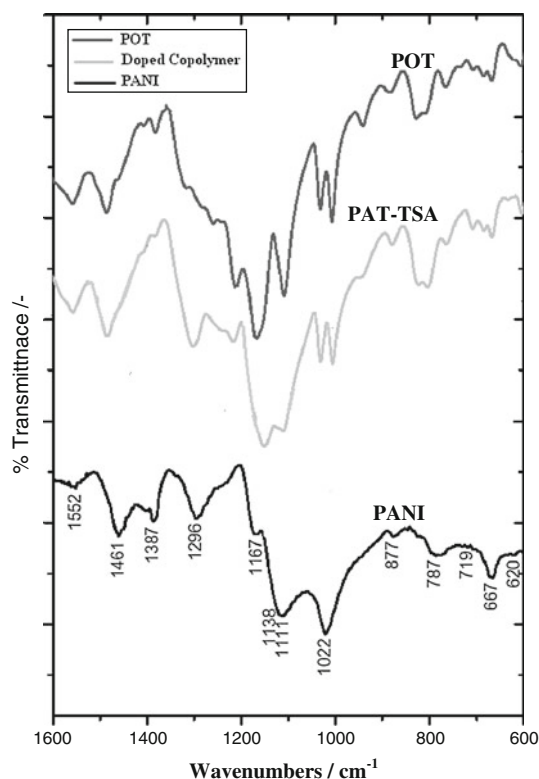

Fig. 1 FTIR spectra of poly (aniline-co-o-toluidine) doped with p-toluene sulphonic acid (PAT-TSA)

spectrum of POT and PAT-TSA due to steric hindrance arising from the methyl group of o-toluidine. The band at 1240 cm^{-1} is not observed in the IR spectrum of a mechanical mixture of PANI and POT. Appearance of a new band clearly indicates the formation of PAT-TSA. A new band of weak to medium intensity corresponding to benzenoid C–N stretching appears at 1240 cm^{-1} in the copolymer. The band at 787 cm^{-1} corresponds to a p-disubstituted benzene ring. The strong band at 1152 cm^{-1} is attributed to the –CH$_3$ rocking mode of copolymer. The band at 1022 cm^{-1} corresponds to S=O stretching mode of the –SO$_3$ group of p-toluene sulphonic acid. The structure of the synthesized copolymer is shown in Fig. 2.

3.2 Weight loss measurements

The corrosion inhibition of mild steel in 0.5 M H$_2$SO$_4$ solution at 25 °C containing various concentrations of the
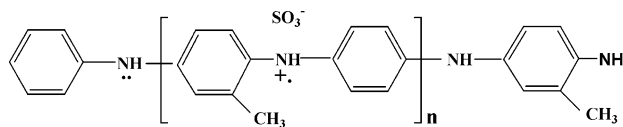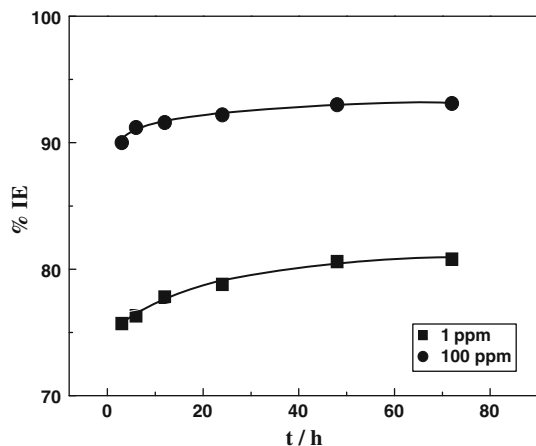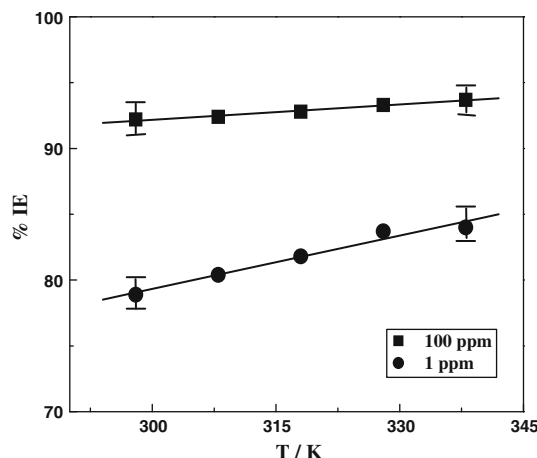

Fig. 2 Structure of PAT-TSA

Table 1 Variation of inhibition efficiency with different concentration of PAT-TSA obtained from weight loss experiments at 25 °C

Concentration (ppm)	Weight loss (mg)	Corrosion rate (mg cm^{-2} h^{-1})	Surface coverage (θ)	IE (%)
Blank	1780	2.920	–	–
1	375.6	0.616	0.789	78.9
5	258.1	0.423	0.855	85.5
10	181.6	0.298	0.898	89.8
50	158.4	0.259	0.911	91.1
100	138.8	0.228	0.922	92.2
150	110.4	0.181	0.938	93.8
200	83.7	0.137	0.953	95.3

PAT-TSA was studied by measuring loss in weight of the mild steel specimen. The data obtained after 24 h of immersion have been recorded in Table 1. The weight loss decreased with increasing inhibitor concentration. The data in the table clearly show an increase in inhibition efficiency from 78.9 to 95.3% as the concentration of PAT-TSA increases from 1 to 200 ppm. The effectiveness of PAT-TSA is due to the presence of lone pair of electrons on nitrogen atoms and delocalized π-electrons of the benzene rings. The variation of inhibition efficiency with immersion time is shown in Fig. 3. It is found that inhibition efficiency increases from 75.7 to 80.8% with increase in immersion time from 3 to 72 h for 1 ppm of inhibitor and from 90 to 93.1% for 100 ppm. The inhibition efficiency beyond 72 h remains almost constant.

The variation of inhibition efficiency with temperature for 1 and 100 ppm of the inhibitor for 24 h of immersion time is shown in Fig. 4. From the figure it is apparent that increase in temperature from 25 to 65 °C causes an increase in inhibition efficiency from 78.9 to 84% at 1 ppm of inhibitor and from 92.2 to 93.7% at 100 ppm. The values

Fig. 4 Variation of inhibition efficiency with different temperatures

of apparent activation energy (E_a) were calculated using Arrhenius equation. A plot of log corrosion rate versus 1/T obtained by weight loss measurement without and with 1 ppm and 100 ppm of the inhibitor gave straight lines (Fig. 5). The value of activation energy (E_a) obtained from the slope of this line is given in Table 2. The values of standard enthalpy of activation (ΔH^0) and standard entropy of activation (ΔS^0) were calculated using the following equation [30]:

$$CR = \frac{RT}{Nh}\exp\left\{\frac{\Delta S^0}{R}\right\}\exp\left\{-\frac{\Delta H^0}{RT}\right\} \tag{6}$$

where CR is the Corrosion rate, h is the Planck's constant, N is the Avogadro number and R is the gas constant. The plot of log (CR/T) versus 1/T yielded straight lines (Fig. 6) with a slope of ($-\Delta H^0/2.303R$) and an intercept of [{log (R/Nh) + ($\Delta S^0/2.303R$)]. The values of enthalpy of activation (ΔH^0) and entropy of activation (ΔS^0) obtained from the slopes and intercepts of these lines are recorded in Table 2. The values of E_a and ΔH^0 are close to each other

Fig. 3 Variation of inhibition efficiency with immersion time of electrode
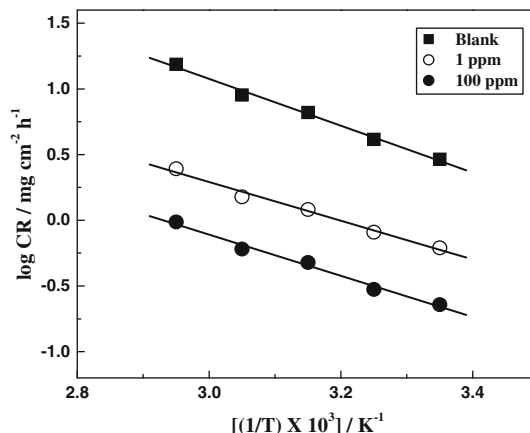
Fig. 5 Arrhenius plots of log of CR versus 1/T at different concentrations of PAT-TSA

Table 2 Thermodynamic activation parameters for mild steel in 0.5 M H_2SO_4 in the presence and in absence of PAT-TSA

Thermodynamic parameters	0.5 M H_2SO_4	PAT-TSA	
		1 ppm	100 ppm
E_a (kJ mol^{-1})	34.16	28.22	30.0
ΔH^0 (kJ mol^{-1})	31.53	25.62	27.3
ΔS^0 (J mol^{-1} K^{-1})	130.53	163.42	166.0
ΔG_{ads} (kJ mol^{-1})	–	55.8	44.8
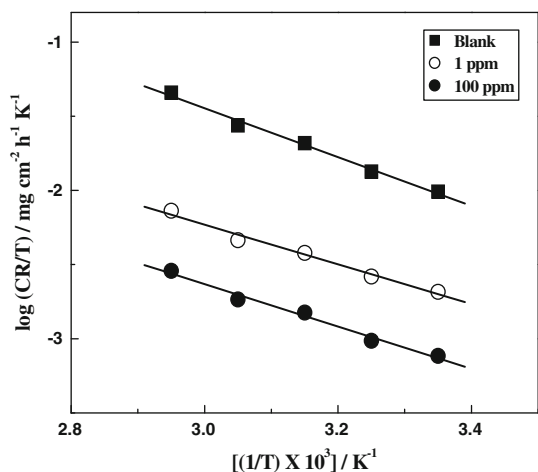
Fig. 6 Arrhenius plots of log of *CR/T* versus 1/*T* at different concentrations of PAT-TSA

and vary in the same manner on the addition of different concentrations of inhibitor. The lower value of the activation energy of the process in the presence of inhibitor as compared to that in its absence is attributed to the chemisorption of the inhibitor [31, 32]. The chemisorption of the inhibitor is also apparent from the higher value of inhibition efficiency at elevated temperatures. Since heat released during chemisorption is utilized for the corrosion process, hence the observed energy of activation apparently becomes smaller. However larger value of energy of activation at higher concentration of the inhibitor indicates that at higher concentrations, the corrosion process is governed by the pre-exponential factor whereas at low concentrations it is controlled by the kinetic parameters of activation [33]. Although the values of ΔS^0 both in the absence and presence of inhibitor are large and negative, these become more negative with successive increase in concentration of the inhibitor. This indicates that the activated complex is more ordered in the presence of the inhibitor [34, 35]. The activated complex could be described as Fe–H$^+$ which on decomposition gives Fe^{2+} and H$_2$. Further, decrease in entropy on the addition of inhibitor is due to the formation of Fe-inhibitor complex which results in the lowering of corrosion rate.
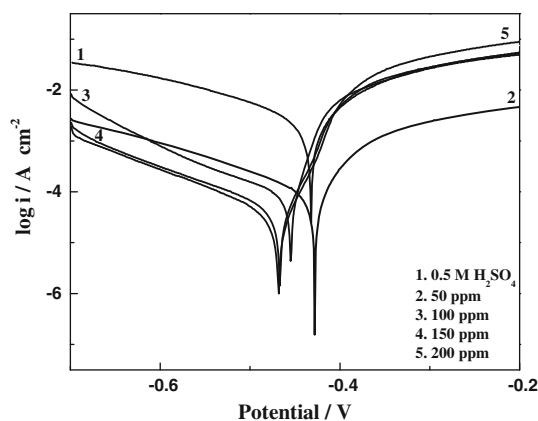
3.3 Potentiodynamic polarization studies

The potentiodynamic polarization behaviour of mild steel in 0.5 M H_2SO_4 containing different concentrations of PAT-TSA at 25 °C is shown in Fig. 7. The corrosion parameters viz. corrosion potential (E_{corr}), the corrosion current density (I_{corr}), anodic Tafel slope (β_a), and cathodic Tafel slope (β_c) derived from these curves are given in Table 3. It is evident from the table that the value of I_{corr} has decreased from 2589 μA cm^{-2} for the blank to 506.4 μA cm^{-2} in presence of 1 ppm of inhibitor and it further reduces to 89.9 μA cm^{-2} as the concentration of inhibitor is gradually increased to 200 ppm. The addition of PAT-TSA does not alter the values of E_{corr} indicating that this is an ambiodic inhibitor. Further, the addition of inhibitor reduces the cathodic current significantly thus decreasing the hydrogen evolution reaction. This suggests that, although the inhibitor is ambiodic in nature, it is predominantly cathodic. It is further supported from the fact that cathodic slope values (β_c) are always greater than the anodic slope values (β_a) indicating predominance of cathodic inhibitors [36].

From the linear polarization studies it has been observed that the polarization resistance R_p increases from 14.4 Ω cm^2 for the blank solution to 422.6 Ω cm^2 for 200 ppm of the inhibitor. The increase in polarization resistance in the presence of the inhibitor suggests that a non-conducting physical barrier is formed at the metal electrolyte interface. This barrier is formed due to the adsorption of PAT-TSA on mild steel surface giving the highest inhibition efficiency of 96.6% at 200 ppm for which the polarization resistance is the highest.

3.4 Electrochemical impedance spectroscopy

The variation in the impedance behaviour of mild steel in 0.5 M H_2SO_4 with the addition of various concentration of


Fig. 7 Potentiodynamic polarization behavior of mild steel in 0.5 M H_2SO_4 with the addition of different concentrations of PAT-TSA at 25 °C

Table 3 Corrosion kinetic parameters of mild steel in 0.5 M H₂SO₄ with different concentrations of PAT-TSA at 25 °C

Concentration (ppm)	E_{corr} (mV vs. Ag/AgCl)	βa (mV dec⁻¹)	βc (mV dec⁻¹)	I_{corr} (µA cm⁻²)	Surface coverage (θ)	IE (%)
Blank	−429	156.1	189.1	2589	–	–
1	−440	111.1	127.2	506.4	0.804	80.4
5	−431	178.5	135.4	441.7	0.830	83.0
10	−437	140.2	219.8	299.6	0.884	88.4
50	−432	150.7	170.7	263.1	0.898	89.8
100	−421	207.5	172.3	227.2	0.912	91.2
150	−429	157.9	167.3	173.4	0.933	93.3
200	−419	149.2	127.2	89.9	0.965	96.5
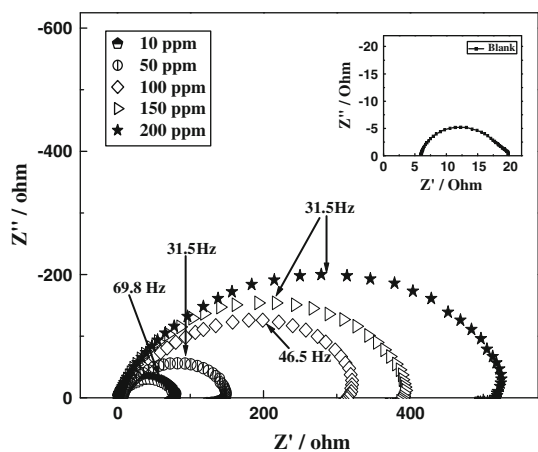
Fig. 8 Nyquist plots of mild steel with the addition of different concentration of PAT-TSA at 25 °C. The figure in the inset refers to the Nyquist plot of the blank solution (0.5 M H₂SO₄)

PAT-TSA is shown in Fig. 8. The existence of a single semicircle shows the presence of a single charge transfer process during dissolution which is unaffected by the presence of inhibitor molecules. The slightly depressed nature of the semi circle which has the center below the x-axis is the characteristic for solid electrodes and such frequency dispersion has been attributed to the roughness and other inhomogeneties of the solid electrode [37, 38]. The surface roughness of the metal is very likely to be caused by metal dissolution during the attainment of open circuit potential. The charge transfer resistance (R_{ct}) and the interfacial double layer capacitance (C_{dl}) values were derived by using the equivalent circuit [39].

The impedance values are given in Table 4. The charge transfer resistance is increased from 14 Ω cm² for inhibitor free solution to 519.9 Ω cm² upon addition of 200 ppm of the PAT-TSA, resulting in 97.3% inhibition efficiency. The increase in R_{ct} value is attributed to the formation of an insulating protective film at the metal/solution interface [40, 41]. The double layer capacitance decreases from 64.7 µF cm⁻² to 9.72 µF cm⁻² in the presence of 200 ppm of PAT-TSA. The initial decrease in C_{dl} value from blank solution to inhibitor containing electrolyte is due to a decrease in the local dielectric constant, while further decrease in C_{dl} with increasing concentrations of the inhibitor is due to increase in the thickness of the electrical double layer [42].

The variation of inhibition efficiency with the concentration of the inhibitor as measured by Tafel extrapolation, weight loss methods and electrochemical impedance has been given in Tables 1, 3 and 4. It can be noted that although the values of inhibition efficiency obtained by different methods are not identical, the difference between

Table 4 Electrochemical impedance and linear polarization parameters for mild steel in 0.5 M H₂SO₄ with different concentrations of PAT-TSA at 25 °C

Concentration (ppm)	Impedance method				LPR method	
	R_{ct} (Ω cm²)	C_{dl} (µF cm⁻²)	IE (%)	Surface coverage (θ)	R_p (Ω cm²)	IE (%)
Blank	14.0	64.7	–	–	14.4	–
1	60.7	38.51	76.9	0.769	79.7	81.9
5	65.8	34.69	78.7	0.787	92.4	84.4
10	75.7	30.16	81.5	0.815	124.2	88.4
50	143.8	23.81	90.3	0.903	132.2	89.1
100	315.8	13.42	95.5	0.955	154.1	90.6
150	398.1	12.69	96.5	0.965	221.8	93.5
200	519.9	9.72	97.3	0.973	422.6	96.6

respective *IE* values is very small and well within the limits of experimental error.

The inhibitive property of water soluble polyaniline prepared by different techniques has been attributed to the presence of plenty of π-electron clouds coexisting with quaternary nitrogen atom [15]. The larger molecular size ensures the greater coverage of the mild steel surface and decreases the effective area for corrosion reaction. With the basic idea of increasing the water solubility and molecular size, polyaniline was copolymerized with *o*-toluidine and doped with *p*-toluene sulphonic acid. In solution form, poly (aniline-co-toluidine) doped with *p*-toluene sulphonic acid is conducting in nature. However the protective barrier formed at the metal solution interface is non-conducting/insulating, as the charges associated with the inhibitor molecules are involved in the bond formation with metal. The *IE* observed in the present study is larger than those obtained by other workers for polyaniline [43] and poly (*p*-toluidine) [44]. In acidic solution, PAT-TSA exists as protonated species. These protonated species were adsorbed on the cathodic sites of the mild steel and decreased the hydrogen evolution reaction. This indicates that the PAT-TSA is a good surface modifier for the corrosion protection of mild steel in H_2SO_4 and acts as a cathodic inhibitor.

3.5 Study of the adsorption isotherm

Basic information on the interaction between the inhibitor and the mild steel surface is provided by the Langmuir adsorption isotherm [45].

$$\frac{C_{inh}}{\theta} = \frac{1}{K_{ads}} + C_{inh} \tag{7}$$

where K_{ads} is the equilibrium constant of the inhibitor adsorption process, C_{inh} is the inhibitor concentration and θ is the fraction of metal surface covered with the inhibitor as a result of adsorption. The surface coverage (θ) of different concentration of inhibitor in acidic media has been evaluated from weight loss experiments for various concentrations of inhibitor as shown in Table 1, using the equation [46]:

$$\theta = \frac{W^0 - W}{W^0} \tag{8}$$

where W and W^0 are the weight loss with and without inhibitor respectively.

The validity of the Langmuir isotherm is confirmed by the linearity of the C_{inh}/θ vs. C_{inh} plot with a slope value close to unity (Fig. 9). The deviation from unity has been described in terms of surface heterogeneity, particularly when corrosion is also occurring simultaneously.

The free energy of adsorption (ΔG_{ads}) at different temperatures was calculated using the following equation [47]:
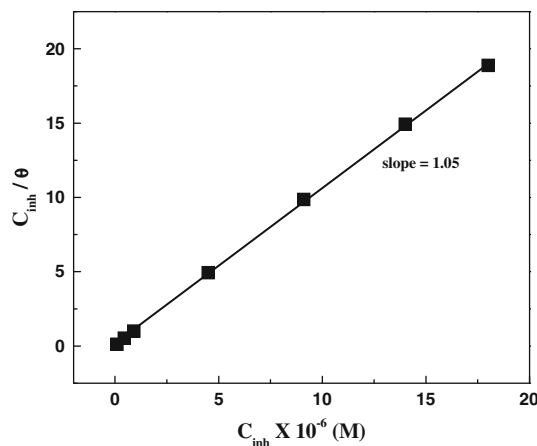
Fig. 9 Langmuir adsorption isotherm plot of mild steel in 0.5 M H_2SO_4 containing different concentrations of PAT-TSA at 25 °C

$$\Delta G_{ads} = -RT \ln(55.5 \, K_{ads}) \tag{9}$$

where 55.5 is the concentration of water in mol l^{-1}. The equilibrium constant for adsorption K_{ads} in the above equation is defined by the relation;

$$K_{ads} = \frac{\theta}{C_{inh}(1 - \theta)} \tag{10}$$

where θ is the degree of coverage on the metal surface. C_{inh} is the concentration of inhibitor in mol l^{-1}. The degree of surface coverage (θ) for the optimum concentration of inhibitor in 0.5 M H_2SO_4 at 25–65 °C for 24 h of immersion time has been evaluated from weight loss values. The negative value of free energy of adsorption indicates spontaneous adsorption of inhibitor molecules on the mild steel surface [48]. Further, the value of ΔG_{ads} being more negative than -40 kJ mol^{-1} shows strong interaction of the inhibitor molecules with the mild steel surface [49], indicating that inhibitor molecules are chemisorbed on the surface.

3.6 Scanning electron microscopy (SEM)

The morphologies of the mild steel surface after corrosion in the presence and absence of inhibitor in 0.5 M H_2SO_4 is shown in Fig. 10. The inhibited metal surface is smoother and more even than the uninhibited surface indicating a protective layer of adsorbed inhibitor preventing acid attack. The SEM photographs of inhibited surface are very similar to those reported earlier [50]. This smooth surface of the metal obtained after corrosion in 0.5 M H_2SO_4 containing 200 ppm of copolymer indicates significant reduction in corrosion rate, due to the formation of a thin layer of copolymer film on the mild steel surface (Fig. 10d–f).
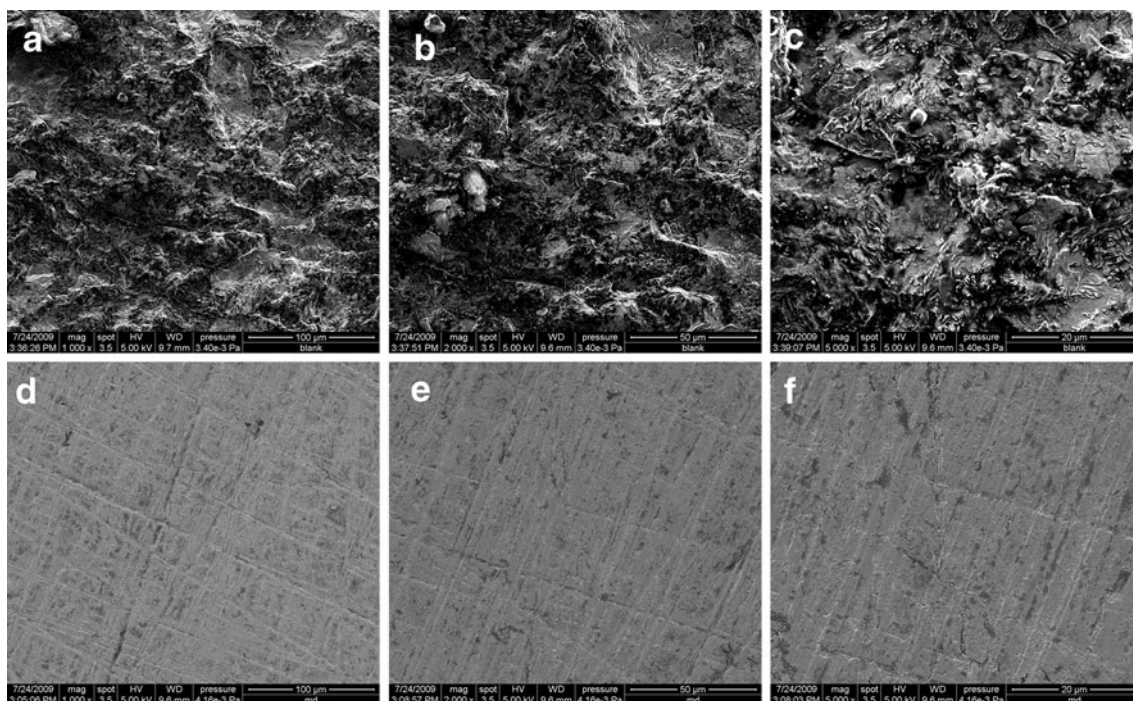
Fig. 10 SEM photographs of the surface of mild steel after 24 h of immersion period at 25 °C in: **a** blank at 1000×, **b** blank at 2000×, **c** blank at 5000×, **d** 200 ppm of PAT-TSA at 1000×, **e** 200 ppm of PAT-TSA at 2000×, **f** 200 ppm of PAT-TSA at 5000×
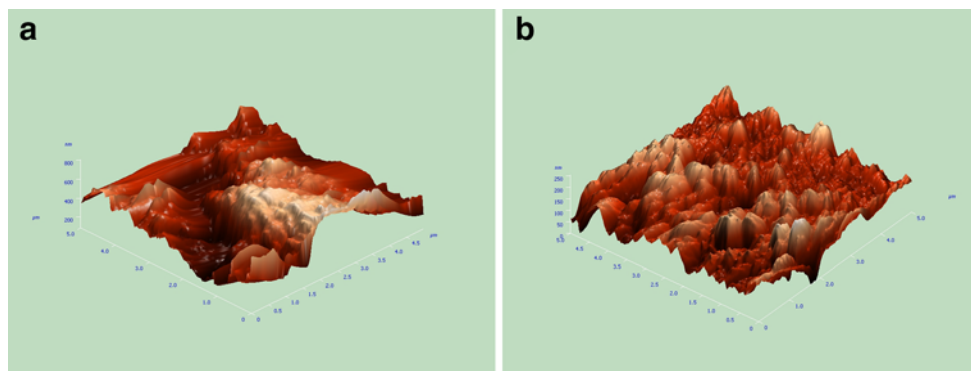
Fig. 11 AFM micrographs of mild steel surface. **a** Blank and **b** 200 ppm of PAT-TSA

The surface morphology of the mild steel specimens was further studied by Atomic Force Microscopy (AFM) before and after corrosion in the presence and absence of synthesized copolymer. The surface morphology supported the formation of an adsorbed copolymer film on the mild steel surface. In Fig. 11a the surface morphology (3D) of the mild steel sample in 0.5 M H_2SO_4 is shown in absence of PAT-TSA. The average roughness was calculated as 117 nm. It is clearly seen from the figure that the steel sample shows a rough surface due to acid corrosion. However, the presence of 200 ppm of PAT-TSA (as inhibitor) retarded the corrosion and the surface of the inhibited mild steel specimen gets smoothened as shown in Fig. 11b. The average surface roughness was calculated as

35 nm, which is probably due to the formation of a copolymer film on the mild steel surface.

4 Conclusion

1. The inhibition efficiency of PAT-TSA increases with increase in inhibitor concentration and approaches 95.3% at 200 ppm.
2. The inhibition efficiency increases with the rise of temperature.
3. The PAT-TSA acts predominantly as a cathodic inhibitor by reducing the area of cathodic site.

4. The adsorption of the synthesized PAT-TSA on the mild steel surface obeys a Langmuir adsorption isotherm.

References

1. Chetouani A, Medjahed K, Sid-Lakhdar KE, Hammouti B, Benkaddour M, Mansri A (2004) Corros Sci 46:2421
2. Achary G, Sachin HP, Arthoba Naik Y, Venkatesha TV (2005) Bull Electrochem 21:241
3. Tamilselvi S, Raman V, Rajendran N (2003) J Appl Electrochem 33:1175
4. Tebbji K, Bouabdellah I, Aouniti A, Hammouti B, Oudda H, Benkaddour M, Ramdani A (2007) Mater Lett 61:799
5. Ali SA, Saeed MT, Rahman SV (2003) Corros Sci 45:253
6. Lagrenee M, Mernari B, Bouanis M, Traisnel M, Bentiss F (2002) Corros Sci 44:573
7. Singh MM, Rastogi RB, Upadhyay BN (1994) Corrosion 50:620
8. Quraishi MA, Sardar R (2002) Corrosion 58:748
9. Singh G, Jha L, Mohapatra R (1990) J Electrochem Soc India 39:4
10. Luo H, Guan YC, Han KN (1998) Corrosion 54:721
11. AbdEl Fattah AA, AbdEl Gulil RM, Megahed HE, AbdEl Haleem SM (1991) Bull Electrochem 7:18
12. Khaled KF, Hackerman N (2003) Electrochem Acta 48:2715
13. Ayers RC Jr, Hackerman N (1963) J Electrochem Soc 110:507
14. Trabanelli G, Zucchi F (1972) Rev Coat Corros 1:97
15. Sathiyanarayanan S, Dhawan SK, Trivedi DC, Balakrishnan K (1992) Corros Sci 33:1831
16. Sathiyanarayanan S, Balakrishnan K, Dhawan SK, Trivedi DC (1994) Electrochim Acta 39:831
17. Jeyaprabha C, Sathiyanarayanan S, Phani KLN, Venkatachari G (2005) Appl Surf Sci 966
18. Jeyaprabha C, Sathiyanarayanan S, Phani KLN, Venkatachari G (2005) J Electroanal Chem 585:250
19. Lee Y, Cui CQ (1996) J Electroanal Chem 403:109
20. Manickavasagam R, Jeya Karthik K, Paramasivam M, Venkatakrishna Iyer S (2002) Anti-Corr Method Mater 49:19
21. Bentiss F, lagrenee M, Traisnel M, Hornez JC (1999) Corros Sci 41:789
22. Jutter K (1990) Electrochem Acta 35:150
23. Tsuru T, Haruyama S, Gijutsu B (1978) J Jpn Soc Corros Eng 27:573
24. Dus B, Szklarska-Smialowska Z (1984) Corrosion (Nace) 15:175
25. Rao PS, Subrahmanya S, Sathyanarayana DN (2002) Synth Met 128:311
26. Rao PS, Sathyanarayana DN, Palaniappan S (2002) Macromolecules 35:4988
27. Wei Y, Hariharan R, Patel SA (1990) Macromolecules 23:758
28. Savitha P, Sathyanarayana DN (2004) Polym Int 53:106
29. Kulkarni MV, Viswanath AK, Mulik UP (2005) Mater Chem Phys 89:1
30. Bockris JO'M, Reddy AKN, (1977) Modern electrochemistry, vol 2. Plenum Press, New York, p 1267
31. Szauer T, Brandt A (1981) Electrochim Acta 26:1209
32. Foroulis ZA (1985) Proceedings of the 6th European symposium on corrosion inhibitors, Ferrara, p 48
33. Bouklah M, Hammouti B, Lagrenee M, Bentiss F (2006) Corros Sci 48:2831
34. Martinez S, Stern I (2002) Appl Surf Sci 199:83
35. Marsh J (1988) Advanced organic chemistry, 3rd edn. Wiley Eastern, New Delhi
36. Saratha R, Priya SV, Thilagavathy P (2009) E-J Chem 6:785
37. Mansfeld F, Kending MW, Tsai S (1982) Corrosion 38:570
38. Pajkossy T (1994) J Electroanal Chem 364:111
39. Mansfeld F (1981) Corrosion 36:301
40. Bentiss F, Traisnel M, Lagrenee M (2000) Corros Sci 42:127
41. Murlidharan S, Phani KLN, Pitchumani S, Ravichandran S, Iyer SVK (1995) J Electrochem Soc 142:1478
42. McCafferty E, Hackermann N, Tsai S (1982) Corrosion 38:57
43. Jeyaprabha C, Sathiyanarayanan S, Venkatachari G (2006) J Appl Polym Sci 101:2144
44. Manivel P, Venkatachari G (2007) J Appl Polym Sci 104:2595
45. Xu F, Duan J, Zhang S, Hou B (2008) Mater Lett 62:4072
46. Landolt D (1993) Corrosion et Chimie de Surface des Metaux, 1st edn. Alden Press, Oxford, p 495
47. Flis J, Zakroczymski T (1996) J Electrochem Soc 143:2458
48. Donahue FM, Nobe K (1965) J Electrochem Soc 112:886
49. Elachouri M, Hajji MS, Salem M, Kertit S, Aride J, Coudert R, Essassi (1996) Corrosion 52:103
50. Baojiao G, Xin Z, Yanling S (2008) Mater Chem Phys 108:375